eprints@whiterose.ac.uk
https://eprints.whiterose.ac.uk/

Journal Name

ARTICLE

The effect of hyperbranched poly(acrylic acid)s on the morphology and size of precipitated nanoscale (fluor)hydroxyapatite

Laura Shallcross,[a,b] Kevin Roche,[c] Caroline J. Wilcock,[b] Kenneth T. Stanton,[c] Thomas Swift,[d] Stephen Rimmer,[d] Paul V. Hatton,[b,*] Sebastian G. Spain[a,*]

Hydroxyapatite and fluorhydroxyapatite (F)HA nanoparticles were synthesised in the presence of branched poly(acrylic acid)s (PAA) synthesised via reversible addition-fragmentation chain transfer polymerisation and compared to those synthesised in the presence of linear PAA. Analysis of the resulting nanoparticles using Fourier transform infrared spectroscopy, powder X-ray diffraction and transition electron microscopy found that polymer was included within the nanoparticle samples and affected their morphology with nanoparticles synthesised in the presence of branched PAA being more acicular and smaller overall.

Introduction

Current challenges involved in the design and preparation of functional nanoparticles include the difficulty of overcoming nanoparticle aggregation. The formation of aggregates is thermodynamically favourable; however, it prevents the full functionality of nanoparticles from being expressed. If the nanoparticles could be dispersed, this would increase their functionality and improve their application to medicine and dentistry. The interaction of calcium phosphates and organic materials at the nanoscale is a subject of great scientific interest as it is relevant to both biological mineralisation processes and the preparation of bioinspired materials for medical and consumer health applications.[1, 2] In bone and tooth tissue mineralisation, biological apatites interact with organic polymers (typically collagen type I or amelogenin respectively) at the molecular and nanoscales to generate functional load bearing structures.[3-6] Research into similar inorganic-organic interactions has also been shown to offer promise in the development of new functional biomaterials[7-10] and new strategies for delivery of therapeutic molecules,[11-16] as well as providing more fundamental insights into the mechanisms that underpin behaviour at the nanoscale and how these might be applied to control the behaviour of materials. Towards this goal, Roche and Stanton recently described the preparation of orientated biomimetic structures through the combination of linear poly(acrylic acid)s (PAA) and nanoscale fluorhydroxyapatite.[17] Additionally, they demonstrated that particle morphology was affected. While this study provided promising data and proposed a mechanism that might account for nanoscale crystal alignment, it was limited to using simple linear polyacids and relatively insoluble fluorhydroxyapatite.

Here we aimed to investigate the interaction of branched poly(acrylic acid)s with both nanoscale hydroxy- and fluorhydroxyapatites, increasing knowledge of the possible mechanisms that drive their interaction and developing a wider range of controlled and bioinspired material systems for further investigation for medical applications. To achieve this, branched poly(acrylic acid)s were synthesised using reversible addition-fragmentation chain-transfer (RAFT) polymerisation and incorporated into the wet precipitation method used by Roche and Stanton.[17] Two RAFT agents were used to synthesise highly branched poly(acrylic acids): 4-vinylbenzyl pyrrolecarbodithioate (VPC) and 4-vinylbenzyl dithiobenzoate (VBD). The resulting materials were compared to those synthesised in the presence of commercially sourced linear PAA of low molecular weight (Versicol E5, M_w = 9 kDa) and high molecular weight (Versicol E11, M_w = 210 kDa) and in the absence of polymer.

It was hypothesised that the inclusion of polymers with different architectures would lead to changes in the morphology and size of hydroxy- and fluorhydroxyapatite structure to create composite organic-inorganic nanoparticles. Characterisation of the synthesised particles via fourier transform infrared spectroscopy (FTIR), X-ray diffraction (XRD), transmission electron microscopy (TEM) and

a. Polymer and Biomaterials Chemistry Laboratories Department of Chemistry, University of Sheffield, Brook Hill, Sheffield, S3 7HF, UK.

b. Bioengineering & Health Technologies Group, School of Clinical Dentistry, University of Sheffield, 19 Claremont Crescent, Sheffield, S10 2TA, UK.

c. School of Mechanical and Materials Engineering, University College Dublin, Belfield, Dublin 4, Ireland

d. School of Chemistry and Forensic Sciences, University of Bradford, Bradford, BD7 1DP, UK.

† Footnotes relating to the title and/or authors should appear here.
Electronic Supplementary Information (ESI) available: DOSY NMR experimental details, specific reagent quantities and additional TEM micrographs.. See DOI: 10.1039/x0xx00000x

thermogravimetric analysis (TGA) was used to determine the effects of the different polymer molecular weights and architectures on the composite particles.

Results and Discussion

Polymer and composite synthesis

Scheme 1. Synthesis of hyperbranched poly(acrylic acid).
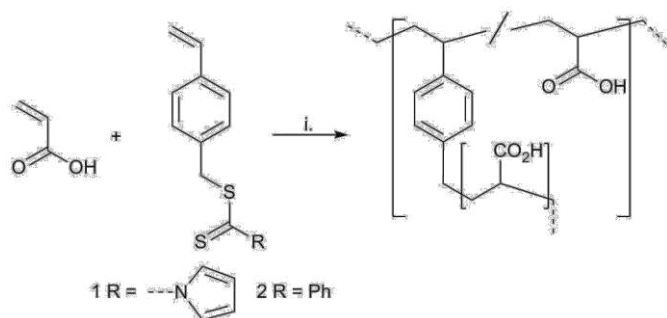
Reagents: i. 4,4'-azobis(4-cyanovaleric acid), dimethylsulfoxide, 60 °C.

Synthesis of hyperbranched poly(acrylic acid): Branched poly(acrylic acid) (PAA) was synthesised via reversible-addition fragmentation chain transfer (RAFT) polymerization using two different RAFT chain transfer agents: 4-vinylbenzyl pyrrole carbodithioate[18] (VPC, **1**) and 4-vinylbenzyl dithiobenzoate[19] (VBD, **2**). RAFT agents were chosen as they have both previously been demonstrated to produce branched polymers and are suitable form the polymerisation of acrylic monomers.[18-20] In both cases 4,4'-azobis(4-cyanovaleric acid) (ACVA) was used as the radical initiator (Scheme 1). Analysis by ^{1}H NMR spectroscopy gave a degree of branching of 0.05 and 0.02 for PAA-VPC and PAA-VBD respectively.[18] ^{1}H NMR spectroscopy was also used to provide a percentage conversion of monomer to polymer with values of 85% for PAA-VPC and 77% for PAA-VBD.

Determination of molar masses and molar mass distributions using size exclusion chromatography proved difficult, with considerable column interactions preventing adequate analysis. In an attempt to reduce column interactions methylation of the acid groups using trimethylsilyldiazomethane[21, 22] was attempted. However, this was also unsuccessful instead resulting in the polymers becoming insoluble in all solvents, as has previously been reported from the methylation of high molar mass PAA.[23] It is believed this was due to the polymer crosslinking during the methylation procedure. As an indication of solution size, radii of gyration (R_g) were determined by diffusion-ordered NMR spectroscopy analysis[24] (see ESI for details) as 2.4 and 4.9 nm for PAA-VPC and PAA-VBD, respectively.

Synthesis of PAA-(fluor)hydroxyapatite composites: Nanoparticles of fluorhydroxyapatite (FHA) and hydroxyapatite (HA) were synthesised according to a literature procedure[25] in the presence of hyperbranched PAAs synthesised using either CTA **1** or **2**. Additionally, (F)HA was synthesised in the presence of commercial linear PAAs with molar masses of 9 kDa (Versicol E5) and 210 kDa (Versicol E11), and the absence of polymer (NoP) for comparison and to act as controls. In all cases the polymer was added to the phosphate solution at 0.2 wt% (~4 wt% of theoretical yield of (F)HA).

Determination of polymer inclusion

Fourier transform infrared spectroscopy: Fourier transform infrared (FTIR) spectroscopy was used to determine inclusion of polymer within the resulting composites, and other effects on the composite structure. Spectra of PAA-(F)HA composites (**Error! Reference source not found.**) showed characteristic bands for both (F)HA and PAA. Additional bands are evident at 1590 and 1450 cm^{-1} for samples containing PAA, and are indicative of the COO[-] asymmetric stretch and CH$_2$ bend for ionised PAA.[26] For PAA-HA samples, the intensity of the OH stretching band (3570 cm^{-1}) is reduced

Figure 1. FTIR spectra of (F)HA synthesised in the presence and absence of linear and branched poly(acrylic acid). Highlighted regions (cm^{-1}): 3570 OH stretch; 1590 COO[-]
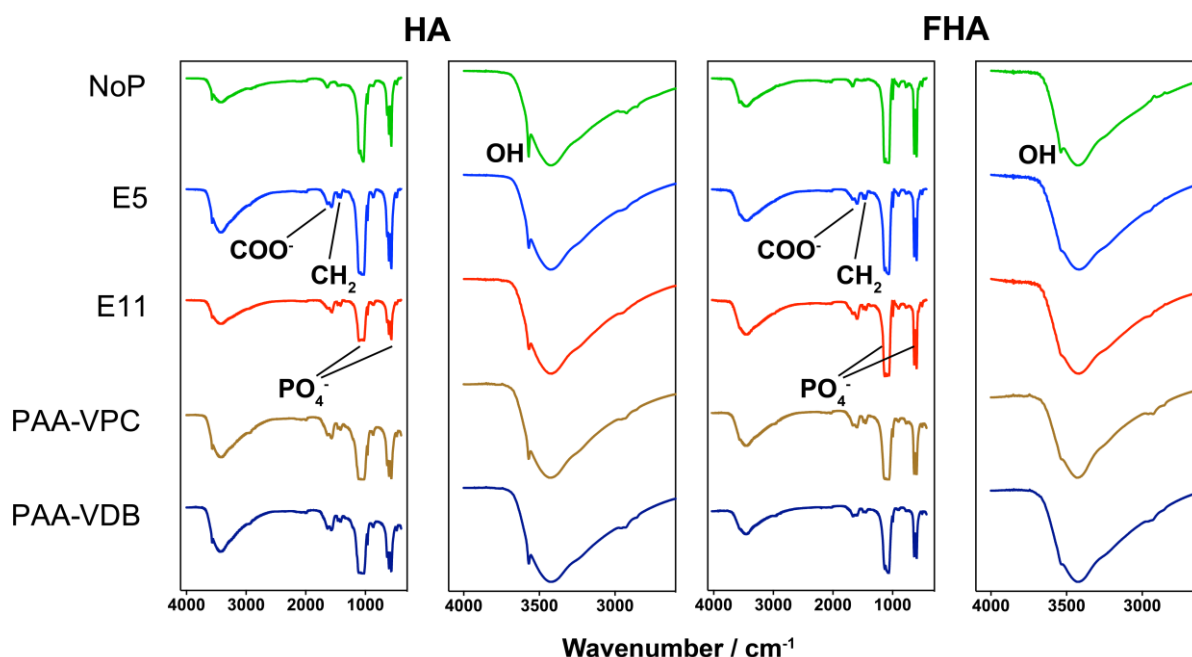
asymmetric stretch; 1450 CH_2 bend; 1030 and 600 PO_4^{3-}.

compared to HA prepared in the absence of PAA, indicating some disruption of the crystal structure and the displacement of some OH groups with PAA.[27] An alternative possibility could be the that PAA potentially interacts with Ca^{2+} ions during precipitation and reduces the amount of Ca^{2+} incorporated into the apatite. To balance the charge of the missing Ca^{2+}, OH^- groups can be replaced with either H_2O or with a vacancy, and some $(PO_4)^{3-}$ groups are replaced with $(HPO_4)^{2-}$ or $(CO_3)^{2-}$ resulting in less order in the crystal.[28] It would be difficult to determine for certain whether this is the case as the vibrations of $(HPO_4)^{2-}$ or $(CO_3)^{2-}$ overlap with the $(PO_4)^{3-}$ and polymer stretching vibrations respectively making them nearly impossible to distinguish from each other.

For FHA-PAA samples (Figure 1), the OH stretching band (3570 cm^{-1}) is almost entirely lost indicating successful incorporation of fluoride. The method used to produce the FHA particles was based on a method by Roche and Stanton where by a targeted fluoride substitution level of 62 % produced a 'real' fluoride incorporation level of 50 %.[29] Additionally, spectra of samples of (F)HA synthesised in the presence of PAA show a reduced intensity in the phosphate bands (1030 and 600 cm^{-1}), again indicating disruption of the crystal structure.
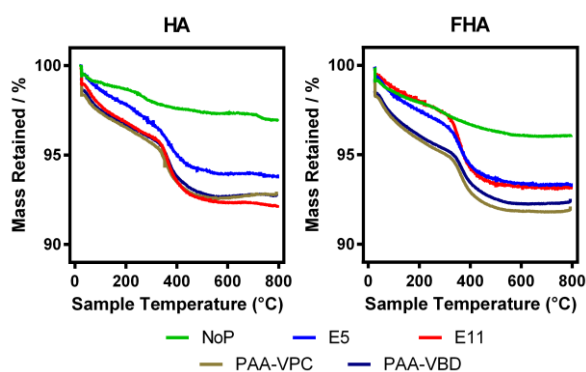

Figure 2. Thermogravimetric analysis of of (F)HA synthesised in the presence and absence of linear or branched poly(acrylic acid)

Thermogravimetric analysis: Thermogravimetric analysis (TGA, **Error! Reference source not found.**) of the composites and control samples was conducted to determine the percentage inclusion of polymer in the composite. The thermogram of the control samples (FHA NoP and HA NoP) displayed a gradual mass loss attributed to residual water and adsorbed carbon dioxide, with <4% total mass loss at 800 °C. For samples containing polymer there is some variation in mass loss below 300 °C and overall. This thought to be due to variation in the quantity of adsorbed carbon dioxide between samples. However, all samples showed a sudden mass loss of 3–4%

between 300 and 360 °C confirming the inclusion of polymer in the composite materials near the theoretical level.

PAA-(F)HA composite morphology and structure
Transmission electron microscopy

Composite morphology, size and dispersion were analysed by transmission electron microscopy (TEM). Micrographs of (F)HA synthesised in the absence of polymer showed lower levels of particle aggregation compared to micrographs of (F)HA synthesis in the presence of both linear and hyperbranched PAA. Such behaviour has been observed previously[25] and is likely due to the charged polymer bridging individual crystallites, resulting in flocculation. However, it cannot be ruled out that this is an artefact of drying in the presence of PAA.

Particle dimensions, and hence aspect ratios, were determined by image analysis using ImageJ.[30] The measurements are summarised in Table 1. The mean crystallite lengths of the FHA samples were shorter than the non-fluorinated HA samples in all cases. This is consistent with literature for intermediate fluoride substitution and is attributed to an increased nucleation rate.[17]

Inclusion of linear PAA (E5 and E11) in HA showed little effect on the crystallite morphology (entries 1–3, Table 1). Conversely hyperbranched PAA (entries 4 and 5, Table 1) showed a decrease in mean length from ~165 nm to 100 nm, and a decreased width from ~22 nm to ~13 nm. Aspect ratios remain similar throughout although HA synthesised in the absence of polymer is the lowest and more plate-like crystallites are evident in the micrographs (**Error! Reference source not found.**). A similar pattern is seen for the FHA samples with the exception of that synthesised in the presence of E11 which shows little change in crystallite length but a reduction in width resulting in an acicular (needle-like) morphology.

Table 1. Crystallite dimensions as determined by image analysis using ImageJ.

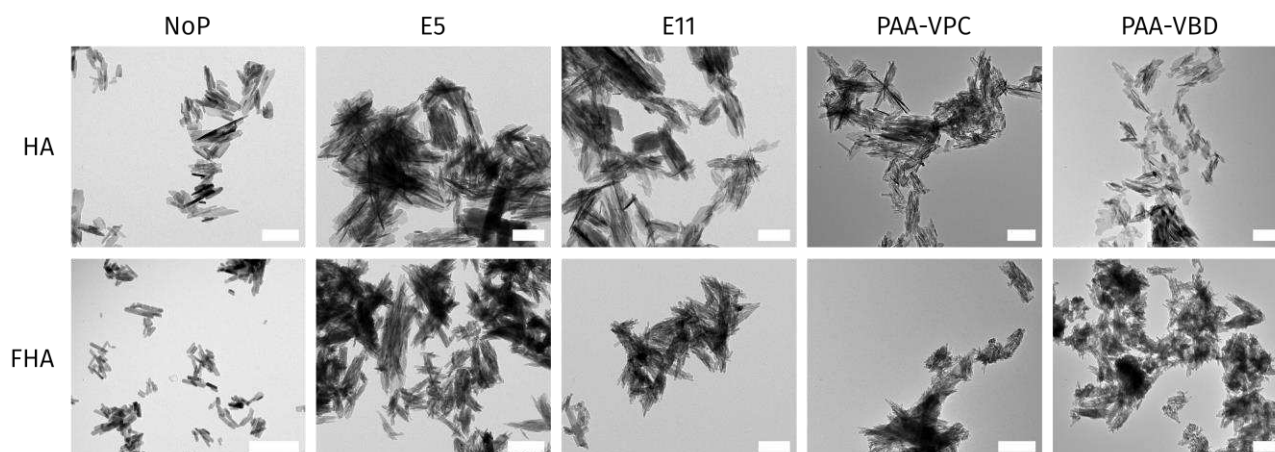| Sample	Width ±SD (nm)	Length ± SD (nm)	l/w
HA NoP	25 ± 12	163 ± 58	6.5
HA E5	22 ± 10	165 ± 56	7.5
HA E11	21 ± 8	168 ± 59	8.0
HA PAA-VPC	12 ± 4	100 ± 27	8.3
HA PAA-VBD	14 ± 6	100 ± 33	7.1
FHA NoP	17 ± 7	81 ± 27	4.8
FHA E5	16 ± 7	89 ± 30	5.6
FHA E11	8 ± 2	93 ± 59	11.6
FHA PAA-VPC	8 ± 3	52 ± 18	6.5
FHA PAA-VBD	9 ± 3	60 ± 20	6.7

Figure 3. Transmission electron micrographs of hydroxyapatite (HA) and fluorhydroxyapatite synthesised in the presence of linear and hyperbranched poly(acrylic acid). Scale bars represent 200 nm
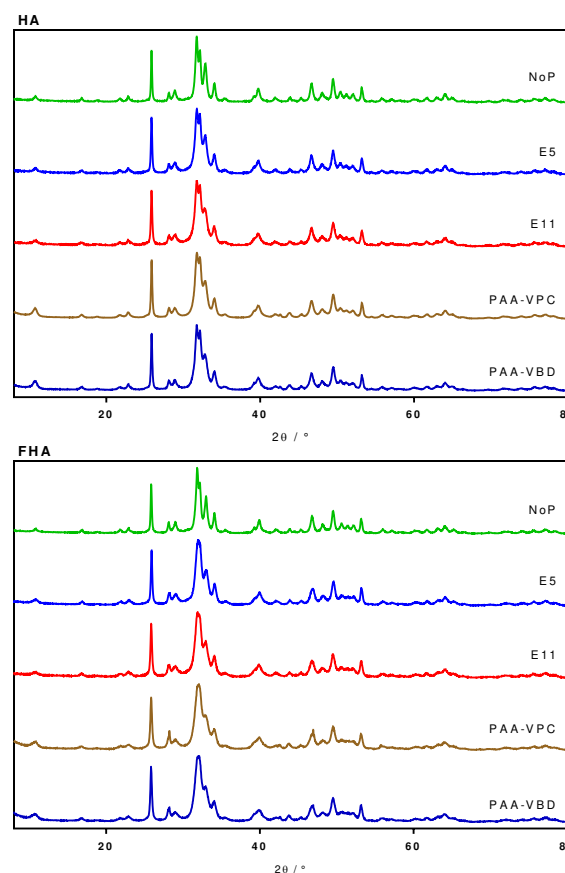
X-ray Powder Diffraction

Composite samples were analysed by X-ray powder diffraction and analysed using an external standard method. Comparison of the diffractograms shows some differences (**Error! Reference source not found.**). Both the HA and FHA samples containing no polymer showed sharper, more intense peaks when compared with samples containing linear and branched polymers indicating a loss of crystallinity and a decrease in particles size when polymer is included in the (F)HA synthesis. This is consistent with inclusion of linear PAA in HA[27] and FHA.[25] Cell parameters were determined by Pawley and Rietveld refinements of the diffraction patterns using the TOPAS (*Total Pattern Analysis Solutions,* Bruker 2009)[31] refinement program. Structure models for HA and FHA were taken from Hughes et al.[32] and the background, unit cell, and size-strain parameters were refined. Calculated parameters are summarised in Table 2.

HA and FHA both have a hexagonal crystal structure with cell parameters $a = b \neq c$. The inclusion of fluoride is evident in the FHA samples with a decrease in cell parameter a of approximately 0.03 Å compared to the non-fluorinated analogues. Cell parameter c is also approximately 0.01 Å larger for fluorinated samples. This is consistent with previously reported values for (F)HA.[17, 32] In samples prepared in the presence of polymer (E5, E11, PAA-VPC and PAA-VBD) there is no evident change in cell parameters compared to the no polymer controls. This is likely due to the fact that the fitting of the data proved difficult due to elongation of peaks at 26° and 53° 2θ corresponding to the 002 and 004 planes respectively in all samples containing polymer.

The difference in the size of the OH$^-$ and F$^-$ ions is evident in the unit cell parameter a values which are larger for all the HA samples than the FHA samples. This is also impacted by rotation of the phosphate groups caused by situation of ions either on the mirror planes (F) or displaced from them (OH).[33]

The small difference in the c parameter values for all samples showed the inclusion of polymer and substitution of OH$^-$ for F$^-$ has a limited effect on the c axis of the unit cell as expected. However, looking at the peak shapes in comparison to those seen when fitted saw far more intense peaks at approximately

26° and 53° 2θ. This suggests that the polymer has been incorporated into the HA to form a composite structure and

caused greater long range order along the c axis than pure FHA or HA.

Figure 4. X-ray powder diffraction patterns for (F)HA synthesised in the presence and absence of linear and branched poly(acrylic acid).

Table 2. Crystallite sizes and cell parameters calculated from X-ray powder diffraction analysis.

Sample	Pawley Refinement		Rietveld Refinement	
	a (Å)^a	c (Å)^a	a (Å)^a	c (Å)^a
HA NoP	9.43(1)	6.87(2)	9.43(1)	6.881(4)
HA E5	9.424(1)	6.87(1)	9.43(1)	6.88(1)
HA E11	9.43(2)	6.87(1)	9.44(1)	6.88(1)
HA PAA-VPC	9.42(1)	6.87(3)	9.43(1)	6.87(1)
HA PAA-VBD	9.42(1)	6.87(1)	9.43(1)	6.87(1)
FHA NoP	9.39(1)	6.881(1)	9.401(4)	6.885(4)
FHA E5	9.38(1)	6.875(2)	9.39(1)	6.88(1)
FHA E11	9.39(1)	6.88(1)	9.40(1)	6.88(1)
FHA PAA-VPC	9.40(1)	6.88(2)	9.39(3)	6.88(3)
FHA PAA-VBD	9.401(2)	6.881(3)	9.40(1)	6.88(1)

^{a} values in brackets are the estimated standard deviation of the last digit

Materials and Methods

Materials

Acrylic acid (Sigma-Aldrich, anhydrous, contains 200 ppm MEHQ as inhibitor, 99%,), and pyrrole (Sigma-Aldrich, 98%) were distilled before use. Anhydrous N,N-dimethylformamide (DMF) and tetrahydrofuran (THF) were obtained using a Grubbs dry solvent system[34] (models SPS 400-6 and SPS200-6). Sodium hydride (Sigma-Aldrich, 60% in mineral oil), carbon disulfide (Sigma-Aldrich, 99.9%), 4-vinylbenzyl chloride (Sigma-Aldrich, 90%), magnesium turnings (Sigma Aldrich, 98%), bromobenzene (Sigma-Aldrich, 99%), calcium hydroxide (Sigma-Aldrich, ≥ 95%), phosphoric acid (Sigma-Aldrich, 85 wt. % in H_2O, 99.99% trace), methanol (Sigma Aldrich, ≥ 99.9%), ethyl acetate (Sigma Aldrich, 99.7%), diethyl ether (VWR Chemicals, anhydrous AnalaR NORMAPUR), acetone (VWR Chemicals, anhydrous AnalaR NORMAPUR), dioxane (Sigma Aldrich, 99.8%) and silica gel (Fluorochem, 35-60 mesh, 60Å) were used as received.

Analytical Methods

Nuclear Magnetic Resonance (NMR) spectroscopy

^{1}H NMR spectra were recorded on a Bruker AV-400 instrument running at 400 MHz at ambient temperature. 20 mg samples were dissolved in deuterated solvent, filtered and placed into a 7 inch NMR tube. Chemical shifts are reported relative to TMS.^{13}C NMR spectra were recorded on a Bruker AV-400 instrument running at 100MHz at ambient temperature. 50 mg samples were dissolved in deuterated solvent, filtered and placed into a 7 inch NMR tube.

Fourier Transform Infrared (FTIR) Spectroscopy

IR Spectra were recorded using a Bruker Vertex 70 spectrometer (Ettlingen, Germany) in the range 400 - 4000 cm^{-1}. 1 mg of the sample was mixed with 50 mg of dried KBr by hand using a pestle and mortar; the mixture was then pressed into a 12 mm diameter disk under a pressure of 60 MPa for 3 minutes. Samples were stored in a desiccator prior to analysis. Sixty-four scans were recorded for each spectrum and all spectra were baseline corrected with the 'Opus'

software package (version 7, Bruker) supplied with the spectrometer. A separate sample of pure KBr was used to create a reference spectrum to establish the background prior to each set of measurements.

Elemental Analysis

The carbon, hydrogen, nitrogen and sulfur content of the RAFT agents were determined using a Perkin-Elmer 2400 CHNS/0 series 2 Elemental Analyser. Approximately 20 mg of sample was combusted completely in excess oxygen and combustion reagent. The levels of each element were detected using a thermal conductivity detector system.

X-ray Powder Diffraction (XRD) Spectroscopy

Dried powder samples were analysed using a Siemens D500 diffractometer (Munich, Germany) with Bragg-Brentano geometry and a CuKα source. and ground into a fine powder using a pestle and mortar. A small amount of Vaseline was placed in a circle on a microscope slide and inserted into the XRD holder. The powder sample was then placed on the Vaseline and smoothed until level using a second microscope slide. Analysis was undertaken using the angular range 20–60 ˚2θ. The step size and time per step were 0.04 ˚ and 3 s respectively. Rietveld refinement was performed on the XRD patterns using the TOPAS refinement program.[35] A separate scan of lanthanum hexaboride (LaB$_6$) was used to calibrate the instrument parameters, which were then fixed for future refinements. The unit cell a-parameter for Si was fixed at 5.43088 Å using Powder diffraction file 00-027-1402: Silicon, 2011 as a reference to allow correction for peak-shift errors.

Transmission Electron Microscopy (TEM)

TEM images were taken using a Philips CM-100 transmission electron microscope operating with an acceleration voltage of 100 kV. Samples were prepared by adding approximately 20 mg of sample to 2 mL ethanol in a small vial, which were then sonicated for 15 minutes. The sonicated mixture was then dropped onto a carbon-coated copper grid using a Pasteur pipette and the ethanol was allowed to evaporate.

Thermogravimetric Analysis (TGA)

Thermogravimetric analysis was conducted using a Perkin Elmer Pyris 1 Instrument. N_2 was used as purge gas with a flow rate of 60 ml/min. Calibration was carried out using the curie points of iron and alumel by burning a 10 mg weight of each solid. Any remaining impurities from previous runs were removed by heating the pan in a flame of a Bunsen burner before running the sample. The software Pyris Manager was used to program the furnace using the following parameters: the temperature was held at 25 °C for 5 minutes and then heated up to 800 °C using intervals of 10 C per minute; finally, the temperature was held at 800 °C for another 5 minutes. The resulting thermograms were analysed using Pyris Manager.

Synthetic Methods

Synthesis of 4-vinylbenzyl pyrrolecarbodithioate (VPC, 1)

Sodium hydride (6.03 g, 0.25 mol) in anhydrous DMF (160 mL) was added to a degassed flask to give a grey suspension. Pyrrole (10.02 g, 0.15 mol) in anhydrous DMF (20 mL) was added drop-wise over 30 minutes to give a yellow foam. The solution was stirred for 30 minutes at room temperature then

cooled to 0 °C with an ice bath. Carbon disulfide (9 mL, 0.15 mol) in anhydrous DMF (20 mL) was added drop-wise over 10 minutes giving a dark red solution. The solution was stirred at 0 °C for 30 minutes then 4-vinylbenzyl chloride (22.27 g, 0.15 mol) in dry DMF (20 mL) was added dropwise over 20 minutes giving a brown solution and the solution was stirred overnight at room temperature. The crude product was extracted using diethyl ether (80 mL) and water (80 mL). The mixture was placed in a separating funnel, the top organic layer was collected and the aqueous layer was washed three times with diethyl ether (3 × 100 mL). The organic extracts were combined, dried over magnesium sulfate and filtered. Diethyl ether was removed *in vacuo* yielding the crude product as a brown oil. The product was isolated via column chromatography eluted with petroleum ether, the first band was collected (Rf 0.78) and removal of the solvent *in vacuo* yielded the desired product as a yellow solid (35.0 g, 0.135 mol) which was stored under nitrogen in the freezer (-18 °C). Elemental analysis found: C, 66.89 %; H, 5.76 %; N, 4.40 %; S, 20.89 %. Expected: C, 64.83 %; H, 5.05 %; N, 5.40 %; S, 24.72 %. ESI-MS expected m/z: 259.3, experimental m/z: 259.0[1]H NMR (400 MHz, CDCl$_3$) δ ppm: 4.60 (s, 2H, SC**H**$_2$Ar), 5.25 – 5.28 (dd, 1H, J = 10.8, 0.6 , **H**$_2$C=CHAr), 5.73 – 5.77 (dd, 1H, J = 17.6, 0.6 **H**$_2$C=CHAr), 6.32 (t, 2H, J = 2.4 N(CH)$_2$(C**H**)$_2$), 6.70 (dd, 1H, J = 17.6, 10.8 H$_2$C=C**H**Ar), 7.37 (q, 4H, J = 6.8 H$_2$C=CH**Ar**), 7.75 (t, 2H, J = 2.4 N(C**H**)$_2$(CH)$_2$). ^{13}C NMR (400 MHz, CDCl$_3$) δ ppm 41.50 (**C**H$_2$), 114.37 (H$_2$**C**=CHBz), 126.01–137.36 (H$_2$C=**C**HBz, H$_2$C=CH**Bz** and C(S)**Py**, multiplet), 199.28 (S**C**(S)Py). ν_{max} / cm^{-1}: 3290 (Py N-C), 2930 (CH$_2$), 2150 and 1980 (N-C(=S)S), 1630 (C=S), 1540 and 1460 (H$_2$C=C), 1290 (Py, C=C), 1030 (S-C=S), 910 (Bz, C=C), 690 (C-S)

Synthesis of 4-vinylbenzyl dithiobenzoate (VDB)

Magnesium turnings (1.80 g, 0.150 mol) were gently heated and stirred under nitrogen for 40 minutes. The flask was left to cool to room temperature, then bromobenzene (7 mL, 0.066 mol) in THF (40 ml) was added dropwise over 30 minutes. The reaction was gently heated to instigate the exothermic reaction; the reaction was cooled using an ice bath as required. A grey solution was formed, which was left to stir for 30 minutes at room temperature. Carbon disulfide (4 mL, 0.066 mol) in THF (30 mL) was then added dropwise over 10 minutes; a reaction colour change of grey to yellow to dark red was observed. The reaction mixture was cooled to 0 °C using an ice bath and stirred for 30 minutes. 4-vinylbenzyl chloride (9.5 mL, 0.067 mol) in THF (30 ml) was added drop-wise over 10 minutes, the solution was allowed to warm to room temperature then stirred overnight. The reaction mixture was quenched using distilled water (80 mL) then the organic product extracted using diethyl ether (80 mL). The solutions were separated and the aqueous layer was washed with diethyl ether (3 × 100 mL). The organic extracts were combined and dried over magnesium sulfate then filtered and the solvent removed *in vacuo* yielding the crude product as a red oil. The crude product was purified by flash column chromatography eluting with ethyl acetate. The solvent was removed *in vacuo* yielding the product as a red oil (10.21 g, 0.037 mol). The product was stored at -18 °C. Found: C, 70.99

%; H, 5.24 %; S, 23.77 %. Expected: C, 71.06 %; H, 5.22 %; S, 23.72 %. Expected m/z: 270.4, experimental m/z: 270.1. ^{1}H NMR (400 MHz, CDCl$_3$) δ ppm 4.58 (s, 2H, SC**H**$_2$Ar), 5.29 – 5.26 (dd, 1H, J = 10.8, 0.6 CH=C**H**$_2$), 5.79 – 5.74 (dd, 1H, J = 17.6, 0.6 CH=C**H**$_2$), 6.72 – 6.67 (dt, 1H, J = 17.6, 2.9 C**H**=CH$_2$), 7.57 – 7.33 (m, 7H, Ar) 8.04 (m, 2H, Ar). ^{13}C NMR (400 MHz, CDCl$_3$) δ ppm 42.24 (**C**H$_2$), 114.40 (H$_2$**C**=CHBz), 126.74 – 144.96 (H$_2$C=CH**Bz**, H$_2$C=**C**HBz and C(S)**Bz**, multiplet), 227.75 (S**C**(S)Bz). ν_{max} / cm^{-1}: 2980 (CH$_2$), 1730 (C=S), 1550–1460, 870 and 760 (Bz, aromatic), 1510 (H$_2$C=C), 1040 (S-C=S), 680 (C-S).

Synthesis of branched acrylic acid polymers using reverse addition fragmentation chain transfer (RAFT) polymerisation

Acrylic acid (AA) was mixed with the appropriate quantity of RAFT agent and initiator in dioxane (30 mL) to give a solution with an initial monomer/RAFT agent ratio of 25/1. The reaction mixture was then transferred to an ampoule (50 mL) and subjected to 4 cycles of freeze-pump-thawing to degas the mixture. The ampoule was flame sealed and placed in a water bath to react at 60 °C for 24 hours. The thickened mixture was removed from the ampoule and precipitated into diethyl ether (500 ml). The solvent was decanted off and the polymer was washed with diethyl ether (100 ml) then dissolved in water and freeze dried to give a flaky powder. PAA-VPC: Yield 86%, ^{1}H NMR (400 MHz, (CD$_3$)$_2$SO) δ ppm: 1.51 (br s, backbone H), 2.20 (br s, backbone H), 6.32 (t, 2H, J = 2.4 N(CH)$_2$(C**H**)$_2$), 7.75 (t, 2H, J = 2.4 N(C**H**)$_2$(CH)$_2$), 12.29 (br s, 1H, COO**H**). PAA-VBD: Yield 93%, ^{1}H NMR (400 MHz, (CD$_3$)$_2$SO) δ ppm 1.51 (br s, backbone H), 2.20 (br s, backbone H), 7.57 – 7.33 (m, 7H, Ar) 8.04 (m, 2H, Ar) 12.26 (br s, 1H, COO**H**).

Synthesis of fluorhydroxyapatite and hydroxyapatite varying poly(acrylic acid) additive

Samples of fluorhydroxyapatite and hydroxyapatite were prepared with 0.2 wt.% solutions of linear poly(acrylic acid) (PAA) with approximate molecular weights of either 9000 Da (E5) or 210000 Da (E11) and branched PAA made with CTA-1 (VPC) and 2 (VBD). Control samples containing no PAA were also synthesised. Masses of chemicals used in each instance can be found in Table S2, the protocol for each synthesis was identical in each instance.

A three necked round bottom flask (250 mL) was fitted with a condenser and a heat probe. The flask was charged with a solution of di-ammonium hydrogen orthophosphate ((NH$_4$)$_2$HPO$_4$, 4 g, 30 mmol) and poly(acrylic acid) 25 % solution of either E5 or E11 (0.8 g, 2x10^{-2} and 1x10^{-3} mmol respectively) in deionised water (100 ml) and heated to boiling while stirring. The solution was then adjusted to pH 10 by the addition of 32 % ammonium hydroxide solution and monitored with a pH probe. A solution of calcium chloride (CaCl$_2$, 5.5 g, 50 mmol) in deionised water (100 ml) was adjusted to pH 10 by the addition of 32 % ammonium hydroxide solution. The calcium solution was then added to the phosphate solution via a peristaltic pump over half an hour forming a milky suspension. The boiling suspension was left to stir for one hour at 85 °C, the heat was then turned off and the solution left to stir for 23 hours at room temperature. The suspension was then centrifuged until the solid had settled, the remaining solution was then decanted off and replaced with fresh

deionised water. This washing step was repeated three times. Half of the sample was then resuspended in deionised water and stored while the other half was placed on a watch glass and dried overnight in an oven at 60 °C. The dried solid was ground in a pestle and mortar into a fine white powder then stored. Ammonium fluoride (NH_4F, 0.23 g, 6 mmol) was included in the initial phosphate solution when synthesising fluorhydroxyapatite. Poly(acrylic acid) was not included in samples of fluorhydroxyapatite and hydroxyapatite (sample name FHA NoP and HA NoP respectively) to act as a control.

Conclusions

Hydroxyapatite and fluorhydroxyapatite particles were synthesised using a wet precipitation method including between 3–4 % poly(acrylic acid)s. Characterisation via TEM showed that the FHA samples were smaller than HA samples while XRD analysis concluded that the *a* parameter of FHA was smaller than HA, while the *c* parameter was longer. This was attributed to the fact that fluoride ions lead to a higher-symmetry, lower volume unit cell in the apatite crystal structure than the hydroxyl ion. Rietveld and Pawley refinement of the XRD diffraction patterns showed the inclusion of polymer in the composite samples caused elongation along the 00l plane. However, the role of the PAA during the crystallisation of (F)HA is not as evident. It is possible that the inclusion of the polymer in the crystallisation acts as a nucleation site and enters the (F)HA crystal structure causing disruption to the crystal lattice. This is consistent with the findings of Bertoni et al.[27] and Füredi-Milhofer et al.[36] that the inclusion of PAA during the synthesis of HA nanoparticles affects the degree of crystallinity and the morphology of the particles.

The inclusion of linear polymers showed little to no effect on the particle morphology, while the hyperbranched samples showed decreased particle lengths and widths. However, the overall aspect ratio remained similar throughout, which was ascribed to an increased nucleation rate.[17] This was the case for both the HA and FHA samples, although the FHA E11 sample produced an increased aspect ratio and micrographs showed acicular particles. The control samples containing no polymer were found to be more crystalline and showed less aggregation than the composite samples. Overall it was determined that fluoride substitution reduced particle size and the inclusion of polymer into the composite samples changed the intrinsic crystal lattice of the apatite crystallites. These observations have important implications for the predictable manufacture of nanoscale HA and FHA with distinctive morphological features, features that in turn have the potential to influence their behaviour in a range of medical device and consumer health products where nanostructured calcium phosphates are used increasingly in combination with polymers.

Acknowledgements

1.   N. Desai, *AAPS J.*, 2012, **14**, 282-295.
2.   V. Uskokovic and T. A. Desai, *J. Biomed. Mater. Res. A*, 2013, **101A**, 1416-1426.
3.   X. Y. Liu and S. W. Lim, *J. Am. Chem. Soc.*, 2003, **125**, 888-895.
4.   M. J. Olszta, X. Cheng, S. S. Jee, R. Kumar, Y.-Y. Kim, M. J. Kaufman, E. P. Douglas and L. B. Gower, *Mat. Sci. Eng. R*, 2007, **58**, 77-116.
5.   X. Yang, L. Wang, Y. Qin, Z. Sun, Z. J. Henneman, J. Moradian-Oldak and G. H. Nancollas, *J. Phys. Chem. B*, 2010, **114**, 2293-2300.
6.   A. G. Fincham, J. Moradian-Oldak and J. P. Simmer, *J. Struct. Biol.*, 1999, **126**, 270-299.
7.   D. Shi, *Introduction to Biomaterials*, Tsinghua University Press, 2006.
8.   H. Xu, L. Cheng, C. Wang, X. Ma, Y. Li and Z. Liu, *Biomaterials*, 2011, **32**, 9364-9373.
9.   P. Willi and C. P. Sharma, *Trends in Biomater. Artif. Org.*, 2012, **26**, 1-2.
10.   M. Stigter, K. de Groot and P. Layrolle, *Biomaterials*, 2002, **23**, 4143-4153.
11.   A. C. A. Wan and J. Y. Ying, *Adv. Drug Del. Rev.*, 2010, **62**, 731-740.
12.   F. Jia, X. Liu, L. Li, S. Mallapragada, B. Narasimhan and Q. Wang, *J. Control. Rel.*, 2013, **172**, 1020-1034.
13.   P. Galvin, D. Thompson, K. B. Ryan, A. McCarthy, A. C. Moore, C. S. Burke, M. Dyson, B. D. MacCraith, Y. K. Gun'ko, M. T. Byrne, Y. Volkov, C. Keely, E. Keehan, M. Howe, C. Duffy and R. MacLoughlin, *Cell. Mol. Life Sci.*, 2012, **69**, 389-404.
14.   M. E. Davis, *Mol. Pharm.*, 2009, **6**, 659-668.
15.   I. Brigger, C. Dubernet and P. Couvreur, *Adv. Drug Del. Rev.*, 2012, **64**, 24-36.
16.   A. Bouladjine, A. Al-Kattan, P. Dufour and C. Drouet, *Langmuir*, 2009, **25**, 12256-12265.
17.   K. J. Roche and K. T. Stanton, *J. Fluorine Chem.*, 2014, **161**, 102-109.
18.   R. Plenderleith, T. Swift and S. Rimmer, *RSC Adv.*, 2014, **4**, 50932-50937.
19.   A. J. Heidenreich and J. E. Puskas, *J. Poly. Sci. A. Poly. Chem.*, 2008, **46**, 7621-7627.
20.   D. J. Keddie, G. Moad, E. Rizzardo and S. H. Thang, *Macromolecules*, 2012, **45**, 5321-5342.
21.   L. Couvreur, C. Lefay, J. Belleney, B. Charleux, O. Guerret and S. Magnet, *Macromolecules*, 2003, **36**, 8260-8267.
22.   E. Kuhnel, D. D. P. Laffan, G. C. Lloyd-Jones, T. Martinez Del Campo, I. R. Shepperson and J. L. Slaughter, *Angew. Chem. Int. Ed.*, 2007, **46**, 7075-7078.
23.   I. Lacík, M. Stach, P. Kasák, V. Semak, L. Uhelská, A. Chovancová, G. Reinhold, P. Kilz, G. Delaittre, B. Charleux, I. Chaduc, F. D'Agosto, M. Lansalot, M. Gaborieau, P.

Castignolles, R. G. Gilbert, Z. Szablan, C. Barner-Kowollik, P. Hesse and M. Buback, *Macromol. Chem. Phys.*, 2015, **216**, 23-37.

24. T. Swift, L. Swanson, M. Geoghegan and S. Rimmer, *Soft Matter*, 2016, **12**, 2542-2549.
25. K. J. Roche and K. T. Stanton, *J. Cryst. Growth*, 2015, **409**, 80-88.
26. D. Belton and S. I. Stupp, *Macromolecules*, 1983, **16**, 1143-1150.
27. E. Bertoni, A. Bigi, G. Falini, S. Panzavolta and N. Roveri, *J. Mater. Chem*, 1999, **9**, 779-782.
28. J. A. M. van der Houwen, G. Cressey, B. A. Cressey and E. Valsami-Jones, *J. Cryst. Growth*, 2003, **249**, 572-583.
29. K. J. Roche and K. T. Stanton, *Journal of Fluorine Chemistry*, 2014, **161**, 102-109.
30. C. A. Schneider, W. S. Rasband and K. W. Eliceiri, *Nat. Meth.*, 2012, **9**, 671-675.
31. Bruker, *DIFFRACplus TOPAS 4.2*, 2009.
32. J. M. Hughes, M. Cameron and K. D. Crowley, *Am. Mineral.*, 1989, **74**, 870-876.
33. D. Haverty, S. A. M. Tofail, K. T. Stanton and J. B. McMonagle, *Phys. Rev. B*, 2005, **71**.
34. A. B. Pangborn, M. A. Giardello, R. H. Grubbs, R. K. Rosen and F. J. Timmers, *Organometallics*, 1996, **15**, 1518-1520.
35. L. Lutterotti, *Nucl. Instrum. Meth. B.*, 2010, **268**, 334-340.
36. H. Füredi-Milhofer and S. Sarig, *Prog. Cryst. Growth Ch.*, 1996, **32**, 45-74.